Rupture of a ferrofluid droplet in external magnetic fields using a single-component lattice Boltzmann model for nonideal fluids

G. Falcucci and G. Chiatti
Department of Mechanical and Industrial Engineering, University of "Roma Tre," Via della Vasca Navale 79, 00146 Rome, Italy

S. Succi
Istituto Applicazioni Calcolo, CNR, V. le del Policlinico 137, 00161 Rome, Italy

A. A. Mohamad and A. Kuzmin
Department of Mechanical and Manufacturing Engineering, Schulich School of Engineering, Calgary, Alberta, Canada T2N 1N4

(Received 28 January 2009; revised manuscript received 23 March 2009; published 21 May 2009)

A nonisotropic tensorial extension of the single-component Shan-Chen pseudopotential Lattice Boltzmann method for nonideal fluids is presented. Direct comparison with experimental data shows that this extension is able to capture relevant features of ferrofluid behavior, such as the deformation and subsequent rupture of a liquid droplet as a function of an externally applied magnetic field. The present model offers an economic lattice-kinetic pathway to the simulation of complex ferrofluid hydrodynamics.

DOI: 10.1103/PhysRevE.79.056706 PACS number(s): 47.11.−j, 47.57.J−, 47.65.Cb

I. INTRODUCTION

Ferrofluids are a special class of colloidal suspensions of nanoscale ferromagnetic materials in a liquid carrier, which respond to the presence of an external magnetic fields by developing an internal magnetic dipole, either aligned (ferro) or counteraligned (antiferro) with the external magnetic field [1,2]. The possibility of magnetic control over their properties is triggering both basic and application-oriented research, such as biomedical applications and targeted drug delivery using magnetic nanoparticles [3]. The motion of magnetic nanoparticles in complex fluids is an important and challenging phenomenon, hardly amenable to a quantitative analysis on purely analytical means. As a result, efficient and robust computational methods for the numerical simulation of their dynamical behavior are constantly in high demand. Over the last decade, a new class of mesoscopic methods based on discrete kinetic theory (lattice Boltzmann, LB for short) have emerged as a powerful tool for the numerical investigation of a broad class of complex flows, including multicomponent and multiphase flows [4,5]. In the recent past, this model has been extended to broader physical scenarios, involving the competition between short-range attraction and midrange repulsion [6–8]. In this paper, we point out that such techniques may find a new set of applications in the domain of ferrohydrodynamics. Lattice Boltzmann models for magnetic fluids date back to the early 90s [9,10], and have since then extended to ferrofluids as well [11–16].

In particular, Ref. [13] introduced an anisotropic extension of the multicomponent Shan-Chen model to describe magnetic interactions. In this work, we show that a simpler (single-component) anisotropic extension of the SC model is capable of reproducing the deformation and subsequent rupture of a magnetic droplet under the effect of an external magnetic field, in quantitative agreement with experimental data. This may open an economic pathway to the application of LB techniques [17] to a broad class of ferrohydrodynamic problems.

II. THEORETICAL BACKGROUND

The standard LB equation with pseudopotential interaction (see below) can be expressed as follows (time step made unit for simplicity):

$$f_i(\boldsymbol{x}+\boldsymbol{c}_i,t+1)-f_i(\boldsymbol{x},t)=-\omega(f_i-f_i^{eq})+F_i(\boldsymbol{x},t), \qquad (1)$$

where f_i is the probability density function of finding a particle at site $\boldsymbol{x}$ at time t, moving along the ith lattice direction defined by the discrete speeds $\boldsymbol{c}_i$, with $i=0,\ldots,b$. In this work we shall refer to a standard nine-speed two-dimensional (2D) lattice, with $b=8$. The left-hand side of Eq. (1) stands for molecular free-streaming, whereas the right-hand side represents the collisional relaxation toward local Maxwellian equilibrium, on a time scale $\tau=1/\omega$. The macroscopic fluid density ρ and velocity $\vec{u}$ are given by $\rho(\boldsymbol{x},t)=\Sigma_{i=0}^{b}f_i(\boldsymbol{x},t)$ and $\rho(\boldsymbol{x},t)\boldsymbol{u}(\boldsymbol{x},t)=\Sigma_{i=0}^{b}\boldsymbol{c}_i f_i(\boldsymbol{x},t)$, respectively. The equilibrium distribution function is given by a low-Mach second-order expansion of a local Maxwellian, namely,

$$f_i^{eq}=w_i\rho\left(1+\frac{1}{c_s^2}\boldsymbol{c}_i\cdot\boldsymbol{u}+\frac{1}{2c_s^4}(\boldsymbol{c}_i\cdot\boldsymbol{u})^2-\frac{1}{2c_s^2}u^2\right). \qquad (2)$$

Finally, the term $F_i=w_i\boldsymbol{F}\cdot\boldsymbol{c}_i/c_s^2$ in Eq. (1) describes the coupling to external fields, as well as intermolecular interactions for the case of nonideal fluids. There are many different ways to implement this term [18]; in the present work we choose the original method proposed by Shan-Chen, namely, a standard shift of the velocity field in the local equilibrium, $f_i^{eq}(\boldsymbol{u})\rightarrow f_i^{eq}(\boldsymbol{u}+\boldsymbol{F}\tau/\rho)$. In the Shan-Chen pseudopotential method, the self-consistent force takes the following form:

$$\boldsymbol{F}=-G\psi(\boldsymbol{x})\sum_{i=0}^{b}w_i\psi(\boldsymbol{x}+\boldsymbol{c}_i)\boldsymbol{c}_i, \qquad (3)$$

where $\psi(\rho)$ is the local pseudopotential governing the intermolecular interactions. The specific expression of $\psi(\rho)$ given by Shan and Chen is the following [4]:

$$\psi = \sqrt{\rho_0}(1 - e^{-\rho/\rho_0}), \tag{4}$$

where ρ_0 is a reference density. The structure of the Shan-Chen force is quite general and elegant: the interaction, whose strength is controlled by the scalar parameter G, is basically a two-point coupling between the pseudopotential (sometimes also interpreted as a generalized density) at a given location $\boldsymbol{x}$, and the same pseudopotential at neighbor locations $\boldsymbol{x}+\boldsymbol{c_i}$. For all its simplicity, this term can be shown to feature the two major ingredients of nonideal fluids, namely, a nonideal equation of state and a nonzero surface tension, both driven by the same interaction parameter G [6]. In particular, separation between a dense and light phase is known to occur beyond a critical threshold $G<G_c=-4$ (negative sign codes for attraction) at $\rho_c=\rho_0 \ln 2$.

A distinctive feature of ferrofluids is their anisotropic behavior, as related to their sensitivity to external magnetic fields [1]. In particular, it is known that magnetic droplets undergo anisotropic deformations in response to an externally applied magnetic field. The microscopic origin of such deformations is fairly nontrivial, involving as it does complex interface physics and, eventually, even the spatial configuration of electronic degrees of freedom [2]. However, at a mesoscopic level, this deformation can be represented by a nonisotropic contribution of the magnetic interaction to the fluid pressure. In particular, for a ferrofluid exposed to a magnetic field $\boldsymbol{B}$ along, say, the x direction, the pressure tensor acquires an unbalance $P_{xx}^{mag}-P_{yy}^{mag}=B^2/2\mu_0$, μ_0 being the magnetic permeability.

Since the Shan-Chen force contributes a nonideal (isotropic) term to the pressure tensor, nonisotropic extensions of the Shan-Chen method prove capable of modeling the presence of a magnetic field [13]. In previous lattice Boltzmann models based on the Shan-Chen scheme, magnetic interactions were associated with additional (multicomponent) lattice population carrying magnetic fields/dipoles. However, to the purpose of describing magnetic coupling to an external field, a simpler *single-component* model can be devised, which requires no additional populations as compared to the nonmagnetic case. For the sake of completeness, we proceed to provide the mathematical details of the procedure.

III. ANISOTROPIC SINGLE-COMPONENT SHAN-CHEN MODEL

To keep full generality, we begin by assuming that the scalar G be replaced by an angle-dependent interaction, with a separate coupling strength, G_i, for each direction. Thus, the Shan-Chen force generalizes to

$$\boldsymbol{F} = -\psi(\boldsymbol{x})\sum_{i=0}^{8} w_i G_i \psi(\boldsymbol{x}+\boldsymbol{c}_i dt)\boldsymbol{c}_i dt, \tag{5}$$

where we have restored the time step dt for dimensional clarity.

By Taylor expanding Eq. (3) up to second order in dt, we find

$$\boldsymbol{F}^0 \simeq \psi(\boldsymbol{x})\sum_i w_i G_i \boldsymbol{c_i}\psi(\boldsymbol{x})dt \equiv \vec{g}_0\psi^2, \tag{6}$$

$$\boldsymbol{F}^1 \simeq \psi(\boldsymbol{x})\sum_i w_i G_i \boldsymbol{c_i}\boldsymbol{c_i}\nabla\psi(\boldsymbol{x})dt^2 \equiv \vec{\vec{g}}_1 \cdot \nabla\frac{\psi^2}{2}, \tag{7}$$

where we have set

$$\vec{g}_0 \equiv \sum_i w_i G_i \boldsymbol{c}_i dt, \tag{8}$$

$$\vec{\vec{g}}_1 \equiv \sum_i w_i G_i \boldsymbol{c}_i \boldsymbol{c}_i dt^2. \tag{9}$$

Clearly, the standard isotropic case, $G_i=G$, delivers the familiar result $\vec{g}_0=\vec{0}$ and $\vec{\vec{g}}_1=G\vec{\vec{I}}$, $\vec{\vec{I}}c_s^2$ being the identity tensor. The volumetric force $\vec{g}_0$ does not come in divergence form, and consequently it does not necessarily contribute to the pressure tensor. As a result, we set it to zero by imposing the usual parity-symmetry condition $G_i=G_i*$, where i^* is the mirror partner of i, i.e., $\boldsymbol{c_i}+\boldsymbol{c_i}*=0$. This leaves us with only four independent G_i's out of the original eight (the rest particle $i=0$ makes no contribution to the force term due its zero-velocity magnitude).

Let us now focus on the contribution to the nonideal pressure tensor componentwise: $P_{xx}=\frac{\psi^2}{2}\Sigma_i w_i G_i c_{ix}c_{ix}$, $P_{xy}=\frac{\psi^2}{2}\Sigma_i w_i G_i c_{ix}c_{iy}$, and $P_{yy}=\frac{\psi^2}{2}\Sigma_i w_i G_i c_{iy}c_{iy}$. With the notation, $G_1=G_3\equiv G_x$, $G_2=G_4\equiv G_y$, $G_5=G_7\equiv G_{xy}$, and $G_6=G_8\equiv G_{yx}$, we obtain the following explicit expressions:

$$P_{xx} = c_s^2\frac{\psi^2}{2}\left[\frac{2}{9}G_x + \frac{1}{18}(G_{xy}+G_{yx})\right], \tag{10}$$

$$P_{yy} = c_s^2\frac{\psi^2}{2}\left[\frac{2}{9}G_y + \frac{1}{18}(G_{xy}+G_{yx})\right], \tag{11}$$

and

$$P_{xy} = c_s^2\frac{\psi^2}{2}\left[\frac{1}{18}(G_{xy}-G_{yx})\right]. \tag{12}$$

It is readily checked that in the case of isotropic G, these reduce to the familiar Shan-Chen expressions $P_{xx}=P_{yy}=c_s^2G\psi^2/2$, $P_{xy}=0$.

With these explicit expressions at hand, we can finally draw a quantitative parallel with a magnetic fluid. As a reference case, let us consider the following set of values $G_x=G_0$, $G_{xy}=G_0$, and $G_y=G_0+\delta G_0$. By equating the extra component due to the nonisotropy to the magnetic pressure, we obtain

$$B^2/2\mu_0 = \delta G_0 c_s^2\psi^2/2. \tag{13}$$

For the case of a magnetic droplet, to be considered here, it is expedient to refer to the dimensionless ratio of magnetic to capillary pressure, known as Bond number,

$$\mathrm{Bo} \equiv \frac{p^{mag}}{p^{cap}} = \frac{\delta G_0 c_s^2\psi^2}{2\sigma/D_0}, \tag{14}$$

where σ is the surface tension and D_0 is the diameter of the unperturbed (circular) droplet. This completes our magnetic analogy. In the sequel, we shall validate it against literature data on the deformation of a magnetic droplet as a function of the Bond number.

TABLE I. Square eccentricity of the deforming droplet as a function of the Bo number.

δG_0	Bo	b	a	e^2
0.005	0.685	20	21	0.093
0.010	1.37	19	22	0.254
0.020	2.74	18	24	0.438
0.030	4.11	17	26	0.572
0.040	5.48	15	28	0.713
0.050	6.85	14	30	0.782
0.060	8.22	12	31	0.850
0.070	9.59	11	35	0.901
0.080	10.96	10	38	0.931
0.090	12.33	9	41	0.952
0.100	13.70	9	44	0.958
0.110	15.07	8	47	0.971
0.120	16.44	7	50	0.980

IV. NUMERICAL RESULTS

Baseline simulations have been performed on a 128×128 square lattice, with periodic boundary conditions. The main input parameters are $\rho_0=1$ and $G_0=-4.9$, corresponding to a surface tension $\sigma_0=0.019$. More specifically, we fix $G_y=G_{xy}=G_{yx}=G_0$ and systematically vary the Bond number by acting upon the parameter $G_x=G_0+\delta G_0$. Initial conditions are set to a constant density $\rho_{in}=\ln 2$, with a random perturbation $\delta\rho \pm 0.01\rho_{in}$. Upon phase separation, the droplet remains stable with density $\rho_l \sim 2.0$ in the liquid state and $\rho_g \sim 0.2$ in the vapor state. In the computation of the Bond number, we thus estimate $\psi^2 \sim (\psi_l^2+\psi_g^2)/2 \sim 0.39$.

As a primary observable, we monitor the square eccentricity of the droplet, $e^2=1-b^2/a^2$, a and b representing the minor and major axis of the droplet, respectively. The square eccentricity $e^2=1-(b/a)^2$ obtained by the simulation is compared with the experimental data, as provided in Ref. [19] (see Table I and Fig. 1).

Experimental data are available up to Bo ~ 5.4. In this range, a quantitative agreement between the simulations and

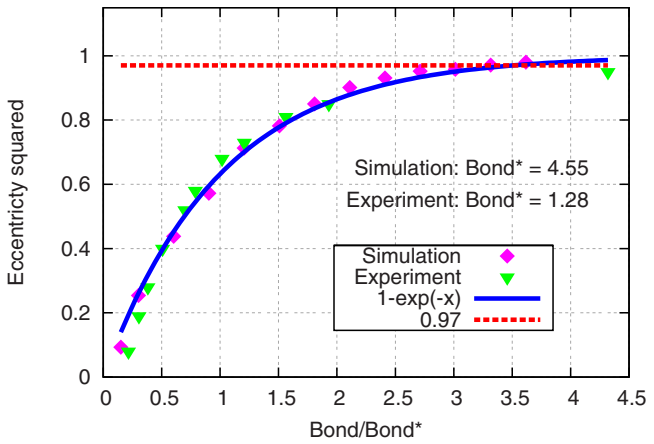

FIG. 1. (Color online) Square eccentricity versus Bond number. LB simulations ($\diamond$), experimental data ($\triangledown$).

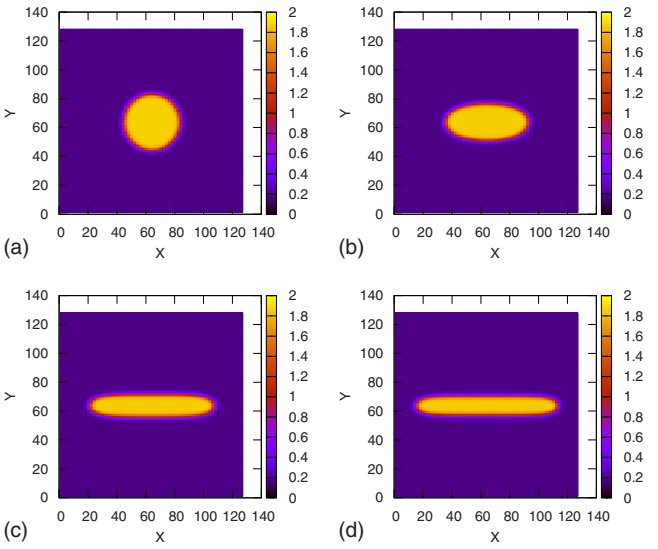

FIG. 2. (Color online) Sequence of density contours illustrating the droplet deformation at increasing Bond number, Bo $=0, 6.84, 13.68, 16.44$. The figures refer to time $t=5000$.

the experimental data is obtained, provided that the square eccentricity is plotted as a function of the rescaled Bond number, $\widetilde{\text{Bo}} \equiv \text{Bo}/\text{Bo}^*$, where $\text{Bo}^* \sim 1.28$ and $\text{Bo}^* \sim 4.55$ are the characteristic Bond numbers resulting from a best fit of the experimental data and the 2D simulations, respectively. In Fig. 1, the simulation results and experimental data are represented, together with the analytical fit, $e^2=1-\exp(-\widetilde{\text{Bo}})$. As one can see, once the Bond number is properly rescaled, both simulations and experimental data fit remarkably well within the same analytical curve. The fact that experimental data exhibit a smaller value of Bo^* as compared to the simulation matches the expectation of a larger propensity to deformation of three-dimensional droplets, with respect to two-dimensional ones. Indeed, the experiments are performed in three dimensions and with a finite aspect ratio $h/D \sim 0.5$, h being the height of the magnetic droplet, while our two-dimensional simulations correspond to an infinite aspect ratio $h/D \to \infty$. Based on the analytical calculations presented in [19], and neglecting the so-called demagnetizing factor (not included in the simulation), at low values of the eccentricity, we can write $e^2 \sim \frac{\chi^2}{3}\frac{2+B^2}{2}\text{Bo}$, where χ is the magnetic susceptibility and $B^{-2}=(1+h^2/D^2)$. From this expression, taking the values $\chi \sim 2.2$ and $B^2=4/5$ for the experiments and $B^2=0$ and $\chi=1$ for the simulations, we obtain $e^2_{(exp)}/e^2_{(sim)} \sim 3.39$, which compares fairly well with the (inverse) ratio of the characteristic Bond numbers $4.55/1.28 \sim 3.55$. The sequence of elliptic droplet configurations at increasing Bond number, is shown in Fig. 2. Simulation data stop at aspect ratios $a/b \sim 7$, beyond which the droplet breaks down (the same limit is observed in Fig. 7 of Ref. [19]). Typical density profiles, together with the corresponding forces, for the case Bo=6.84 and Bo=16.44, are shown in Fig. 3.

Grid independence of our results has been tested. By running at different grid resolutions (64^2 to 256^2) at Bond numbers below the rupture limit, the results do not change for more than a few percent.

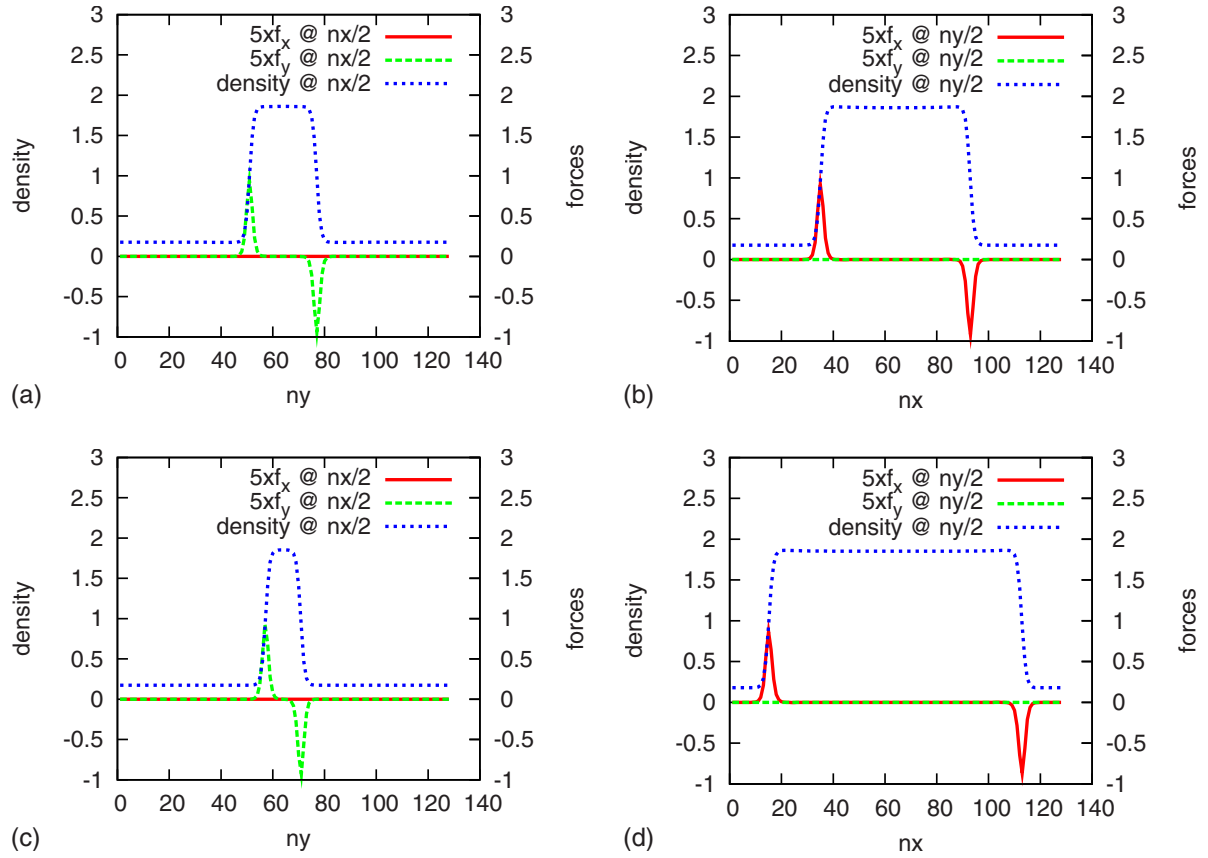

FIG. 3. (Color online) Density cuts across the droplet centerlines along the x and y directions, and corresponding forces at Bo=6.84 and Bo=16.44, at time $t=5000$. The force is magnified by a factor 5 for presentation purposes; $nx=ny=128$ are the domain dimensions.

In order to assess the stability of the elliptical droplet toward further increases in the magnetic field, we have also investigated the region Bo$>$16.5. Simulations have been conducted on up to 10^5 time steps, corresponding to hundreds of magnetic times, $t_{mag}=D/c_A$, $c_A=B/\sqrt{2\mu_0\rho}$ being the Alfven speed.

At Bo=32, we have not been able to find any stable elliptic configuration of the droplet. At Bo=48, the droplet was found to break down into a wormlike structure, which is highly reminiscent of the dumbbell configurations observed in the experiments [19] (see Fig. 4). To inquire the nature of these configurations, we have repeated the simulation with 1024^2 grid points and the same Bond number, Bo$\sim$48, as in the 128^2 grid. The qualitative picture (not shown for space limitations) is basically the same as in the 128^2 grid, although a one-to-one correspondence cannot be expected since we are dealing with unstable structures. By further increasing the magnetic field, the experiments report evidence of multibranched fine-scale structures [19], (see also [1], p. 211). Simulations at Bo=383, with droplets of diameter $D=320$ on a 1024^2 grid, show indeed the emergence of multi-

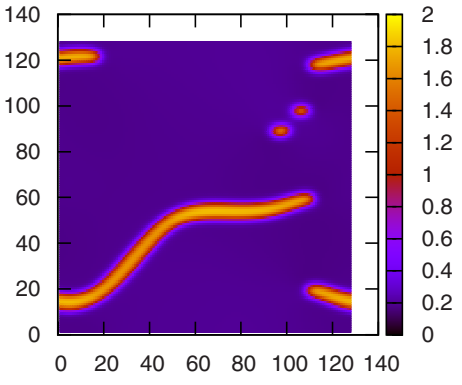

FIG. 4. (Color online) Density contours after the rupture of the droplet, corresponding to $G_0=-4.55$ and $\delta G_0=0.35$, corresponding to Bo$\sim$48. The snapshot refers to time $t=5000$.

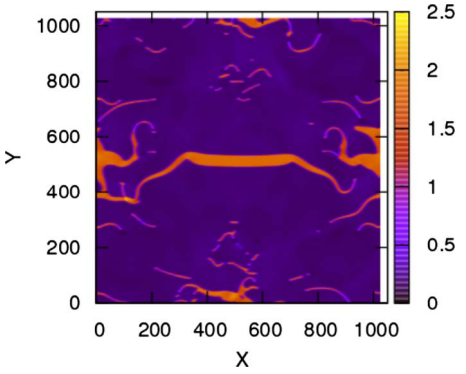

FIG. 5. (Color online) Density contours at time $t=5000$, after the rupture of the droplet, corresponding to $G_0=-4.55$ and $\delta G_0=0.35$ on a 1024^2 grid, corresponding to Bo=383. The onset of fine-scale branched structures is clearly visible.

branched structures, qualitatively similar to the experimental ones (see Fig. 5). A quantitative investigation of such fascinating instabilities requires systematic studies at high spatial resolution and will make the object of future research.

V. CONCLUSIONS

Summarizing, we have presented a nonisotropic extension of the single-component Shan-Chen model for nonideal fluids, which is capable of modeling the deformation of a magnetic droplet, in quantitative agreement with experimental data. The model also shows the emergence of multilevel branched structures, in the unstable regime after the droplet break-up; at high values of the Bond number ($\mathrm{Bo} > 16.5$), the simulated structures appear to be qualitatively similar to the ones observed in the experiments. It is hoped that the present model may open an efficient pathway to the application of LB techniques to the study of complex ferromagnetic fluid phenomena, such as the development of labyrinthine instabilities [20], the motion of ferrofluid droplets in space-time changing magnetic fields [21], as well as to practical applications, such as targeted drug delivery via magnetic nanodroplets [3].

ACKNOWLEDGMENTS

A.K. thanks the Alberta Ingenuity Fund for their financial support. S.S. is grateful to the Killam Foundation for financial support over repeated visits to the University of Calgary, where this work was initiated.

[1] R. E. Rosenweig, *Ferrohydrodynamics* (Cambridge University Press, Cambridge, 1995).
[2] in *Ferrofluids: Magnetically Controllable Fluids and Their Applications*, edited by S. Odenbach (Springer-Verlag, Berlin, 2002); S. W. Charles, in *Ferrofluids: Magnetically controllable fluids and their applications*, edited by S. Odenbach (Springer-Verlag, Berlin, 2002), pp. 3–18; B. Berkovsky and V. Bashtovoi, *Magnetic fluids and Application handbook* (Begell House, New York, 1996).
[3] T. Neuberger, B. Schopf, H. Hoffmann, M. Hoffman, and B. Rechenberg, J. Magn. Magn. Mater. **293**, 483 (2005).
[4] X. Shan and H. Chen, Phys. Rev. E **47**, 1815 (1993).
[5] M. R. Swift, E. Orlandini, W. R. Osborn, and J. M. Yeomans, Phys. Rev. E **54**, 5041 (1996).
[6] M. Sbragaglia, R. Benzi, L. Biferale, S. Succi, K. Sugiyama, and F. Toschi, Phys. Rev. E **75**, 026702 (2007).
[7] G. Falcucci, S. Chibbaro, S. Succi, X. Shan, and H. Chen, EPL **82**, 24005 (2008).
[8] G. Falcucci, G. Bella, G. Chiatti, S. Chibbaro, M. Sbragaglia, and S. Succi, Comm. Comp. Phys. **2**, 1071 (2007).
[9] S. Succi, R. Benzi, and M. Vergassola, Phys. Rev. A **43**, 4521 (1991).
[10] S. Chen, H. Chen, D. Martinez, and W. Matthaeus, Phys. Rev. Lett. **67**, 3776 (1991).
[11] P. J. Dellar, J. Comput. Phys. **179**, 95 (2002).
[12] P. J. Dellar, J. Stat. Phys. **121**, 105 (2005).
[13] V. Sofonea, Europhys. Lett. **25**, 385 (1994).
[14] V. Sofonea and W. J. Frueh, Eur. Phys. J. B **20**, 141 (2001).
[15] V. Sofonea, W. G. Frueh, and A. Cristea, J. Magn. Magn. Mater. **252**, 144 (2002).
[16] M. Hirabayashi, Y. Chen, and H. Ohashi, Phys. Rev. Lett. **87**, 178301 (2001).
[17] R. Benzi, S. Succi, and M. Vergassola, Phys. Rep. **222**, 145 (1992).
[18] Z. Guo, C. Zheng, and B. Shi, Phys. Rev. E **65**, 046308 (2002).
[19] C. Flament, S. Lacis, J. C. Bacri, A. Cebers, S. Neveu, and R. Perzynski, Phys. Rev. E **53**, 4801 (1996).
[20] A. Cebers, Phys. Rev. Lett. **92**, 034501 (2004); S. Banerjee, M. Fasnacht, S. Garoff, and M. Widom, Phys. Rev. E **60**, 4272 (1999).
[21] F. Elias, C. Flament, and J. C. Bacri, Phys. Rev. Lett. **77**, 643 (1996).